

Alma Mater Studiorum Università di Bologna
Archivio istituzionale della ricerca

Photophysics of Deoxycytidine and 5-Methyldeoxycytidine in Solution: A Comprehensive Picture by Quantum Mechanical Calculations and Femtosecond Fluorescence Spectroscopy

This is the final peer-reviewed author's accepted manuscript (postprint) of the following publication:

Published Version:

Martá-nez-fernández, L., Pepino, A.J., Segarra-martá-, J., Jovaiãjaitei, J., Vaya, I., Nenov, A., et al. (2017). Photophysics of Deoxycytidine and 5-Methyldeoxycytidine in Solution: A Comprehensive Picture by Quantum Mechanical Calculations and Femtosecond Fluorescence Spectroscopy. JOURNAL OF THE AMERICAN CHEMICAL SOCIETY, 139(23), 7780-7791 [10.1021/jacs.7b01145].

Availability:

This version is available at: <https://hdl.handle.net/11585/610697> since: 2021-03-14

Published:

DOI: <http://doi.org/10.1021/jacs.7b01145>

Terms of use:

Some rights reserved. The terms and conditions for the reuse of this version of the manuscript are specified in the publishing policy. For all terms of use and more information see the publisher's website.

This item was downloaded from IRIS Università di Bologna (<https://cris.unibo.it/>).
When citing, please refer to the published version.

(Article begins on next page)

This is the final peer-reviewed accepted manuscript of:

Photophysics of Deoxycytidine and 5-Methyldeoxycytidine in Solution: A Comprehensive Picture by Quantum Mechanical Calculations and Femtosecond Fluorescence Spectroscopy

L. Martínez-Fernández, A. J. Pepino, J. Segarra-Martí, J. Jovaišaitė, I. Vaya, A. Nenov, D. Markovitsi, T. Gustavsson, A. Banyasz, M. Garavelli, and R. Improta

***Journal of the American Chemical Society* 2017 139 (23), 7780-7791**

The final published version is available online at :
<http://dx.doi.org/10.1021/jacs.7b01145>

Rights / License:

The terms and conditions for the reuse of this version of the manuscript are specified in the publishing policy. For all terms of use and more information see the publisher's website.

This item was downloaded from IRIS Università di Bologna (<https://cris.unibo.it/>)

When citing, please refer to the published version.

The Photophysics of Deoxycytidine and 5-methyl-deoxycytidine in Solution: a comprehensive picture by Quantum Mechanical Calculations and Femtosecond Fluorescence Spectroscopy.

L. Martínez-Fernández,¹ A. J. Pepino,² J. Segarra-Martí,³ J. Jovaišaitė,⁴ I. Vaya,^{4†} A. Nenov,² D. Markovitsi,⁴ T. Gustavsson,⁴ A. Banyasz,^{4*} M. Garavelli,^{2*} R. Improta^{1,4*}

1. Istituto di Biostrutture e Bioimmagini, CNR, Via Mezzocannone 16, I-80134 Napoli, Italy.

2. Dipartimento di Chimica Industriale “T. Montanari”, Università di Bologna, Viale Risorgimento 4, I-40136 Bologna, Italy.

3. Univ Lyon, ENS de Lyon, CNRS, Université Lyon 1, Laboratoire de Chimie UMR 5182, F-69342 Lyon, France.

4. LIDYL, CEA, CNRS, Université Paris-Saclay, F-91191 Gif-sur-Yvette, France

KEYWORDS (Word Style “BG_Keywords”). DNA, solvent effect, Fluorescence Upconversion, CASPT2/MM, TD-DFT.

ABSTRACT: The study concerns the relaxation of electronic excited states of the DNA nucleoside Deoxycytidine (dCyd) and its methylated analogue 5-methyl-deoxycytidine (5mdCyd), known to be involved in the formation of UV-induced lesions of the genetic code. Due to the existence of four closely lying and potentially coupled excited states, the deactivation pathways in these systems are particularly complex and have not been assessed so far. Here, we provide a complete mechanistic picture of the excited state relaxation of dCyd/5mdCyd in three solvents, water, acetonitrile, and tetrahydrofuran by combining femtosecond fluorescence experiments, addressing the effect of solvent proticity on the relaxation dynamics of dCyd and 5mdCyd for the first time, and two complementary Quantum Mechanical approaches (CASPT2/MM and PCM/TD-CAM-B3LYP). The lowest energy $\pi\pi^*$ state is responsible for the sub-ps lifetime observed for dCyd in all the solvents. In addition, computed Excited State Absorption and Transient IR spectra allow, for the first time, to assign the tens-of-ps time constant, reported previously, to a dark state ($n_o\pi^*$) involving the carbonyl Lone Pair. A second low-lying dark state, involving the Nitrogen Lone Pair ($n_N\pi^*$), does significantly participate in the excited state dynamics. 267 nm excitation of dCyd leads to a non-negligible population of the second bright $\pi\pi^*$ state, which affects the dynamics acting mainly as a ‘doorway’ state for the $n_o\pi^*$ state. The solvent plays a key role governing the interplay between the different excited states; unexpectedly, water favors population of the dark states. In the case of 5mdCyd, an energy barrier present on the main non-radiative decay route explains the six-fold lengthening of excited state lifetime compared to dCyd, observed for all the examined solvents. Moreover, C5-methylation destabilizes both $n_o\pi^*$ and $n_N\pi^*$ dark states, thus preventing them to be populated.

1. INTRODUCTION.

The remarkable photostability of DNA¹ is likely one of the reasons for its selection to store genetic information. Purine and pyrimidine nucleobases, responsible for the strong UV absorption of DNA between 200 and 300 nm, are photostable and characterized by very low ($\sim 10^{-4}$) fluorescence quantum yields and short excited state lifetimes (see below), indicating that non-radiative harmless decay routes can effectively dissipate into heat the energy deposited on the molecules by UV excitation.^{2,3} Due to the biological relevance of these processes, a sheer number of experimental and computational studies have been devoted in the past decade to elucidate the excited state decays of nucleobases and polynucleotides, enabling significant advances in our knowledge of their photoactivated dynamics.⁴⁻⁹ On the other hand, not only for polynucleotides but also for isolated bases in solution, several basic issues require important assessments. Cytosine (Cyt, Figure 1) is the nucleobase with the most debated excited state decay mechanism, and the dis-

agreement does not concern minor details, as for the other bases, but also the main features of the deactivation route. Just to mention some of the most relevant open issues (see section 3.1.2 and SI for a more detailed discussion) all Quantum Mechanical (QM) calculations show that for Cyt four different excited states, corresponding to two bright $\pi\pi^*$ and two dark $n\pi^*$ transitions, fall between 4.5 and 6.0 eV, *i.e.* in the region of the two lowest energy UV absorption bands (see Figure 2), and could be coupled.¹⁰⁻¹⁴ At least three different potentially accessible conical intersections (CoIn) with the ground state (S_0) have been documented, and there is still debate on the preferential non-radiative decay route.^{11,14-20} There are strong experimental indications that a significant amount of the photo-excited population is transferred to one of the two dark excited states, which, however, has not yet been unambiguously assigned.²¹⁻²⁷ Moreover, the substituent effect on cytosine is also an important issue. For example, up to *ca.* 5% of cytosine may be methylated in the human genome and 5-methyl-cytosine plays such an important epigenetic role that it is often referred as the, mobile, fifth base of

DNA.²⁸⁻³⁰ C5-methylation significantly alters the photoactivated dynamics of solvated cytosine, leading to a remarkable increase of the excited state lifetimes.^{24,25,31} The factors responsible for this increase have never been fully disclosed, though this feature could contribute to the larger photoreactivity of 5mdCyd in photodimerization,^{32,33} possibly related to a significant involvement of this base in carcinogenesis.³⁴⁻³⁷ In short, we are in the presence of complex decay pathways and, despite the application of different Time Resolved (TR) spectroscopies, there are several important aspects that remain obscure, for example the effect of solvent proticity, which strongly modulates the excited dynamics of uracil derivatives³⁸ and it has not been tackled so far. Moreover, whereas many computational studies of cytosine and its derivatives in the gas phase (GP) are available,^{11,13,14,39-45} the number of studies in solution is more limited,^{12,46,47} and, to the best of our knowledge, no comprehensive mechanistic study of the excited state decay of deoxycytidine (hereafter, simply, dCyd) and 5-methyl-deoxycytidine (5mdCyd) in solution has been published to date.

The objective of this paper is to achieve a complete description of the excited state deactivation pathways both in dCyd and 5mdCyd. To this end, we study their photoactivated dynamics in three different solvents, water (WAT), acetonitrile (ACN), and tetrahydrofuran (THF), combining femtosecond fluorescence upconversion (FU) experiments and static QM calculations, with two fully complementary computational approaches. For all solvents considered, the two molecules have been studied by TD-CAM-B3LYP calculations, including solvation effects by the polarizable continuum model (PCM).^{48,49} In addition, in the case of water, we consider four water molecules of the first solvation shell (see Figure 1). Photoinduced deactivation routes in aqueous solution, the most biologically relevant environment, were also mapped for the first time resorting to a hybrid MS-CASPT2/MM scheme employing multireference dynamically correlated energies and gradients, and accounting explicitly for solvation and substitution effects. A large number of solvent molecules were explicitly included in the calculation using a classical force field (adopted also for the sugar). Besides interpreting the new FU results, we have also computed the Excited State Absorption (ESA) and the Transient Infra-Red (TIR) spectra from the most relevant stationary and pseudo-stationary points of Potential Energy Surface (PES) of the four lowest energy excited states. We shall focus exclusively on the singlet excited states. Triplet states, which could play an important role in the gas phase,¹⁸ are indeed produced with extremely small quantum yields in solution, both in water⁵⁰⁻⁵² [quantum yield $\sim 10^{-2}$] and in non-polar solvents as chloroform.²⁶

After summarizing the experimental and computational details, in the first subsection of the Results section, we shall report the steady-state absorption and fluorescence spectra of dCyd and 5mdCyd in the three different solvents examined and also FU decays in WAT and ACN. Then, we review the most relevant experimental results available in the literature and introduce the four lowest energy excited states in the Frack-Condon (FC) region according to our calculations. On this ground it will be easier to grasp the significant open issues in dCyd photophysics. Subsequently, we characterize the PES of the four lowest excited states in all solvents, locating their stationary points and crossing regions for both dCyd (section 3.2 and 3.3) and 5mdCyd (section 3.4). The

computed ESA and IR spectra are reported in section 3.5. In the last sections we sketch a general mechanism for the photoactivated decay of dCyd and 5mdCyd, explicitly addressing the main open issues.

Our experiments show that although the steady-state absorption and fluorescence spectra change significantly when going from polar, protic to polar non-protic solvent, the lifetime of the bright states is only slightly modulated. For the first time, we can provide a detailed and comprehensive picture of the excited state decay of dCyd, explaining the effect of C5-methylation. We show that the most significant ultrafast non-radiative decay channel involves an ‘ethene-like’ CoIn between the lowest energy $\pi\pi^*$ excited state and S_0 , whereas other crossings are much less relevant. For dCyd this path is barrierless whereas for 5mdCyd it features a sizeable energy barrier, explaining the longer excited state lifetime compared to dCyd. In dCyd, the second bright excited state plays an important role, being the main ‘doorway’ state for the population of the dark excited state, which is unambiguously identified as that involving the carbonyl Lone Pair.

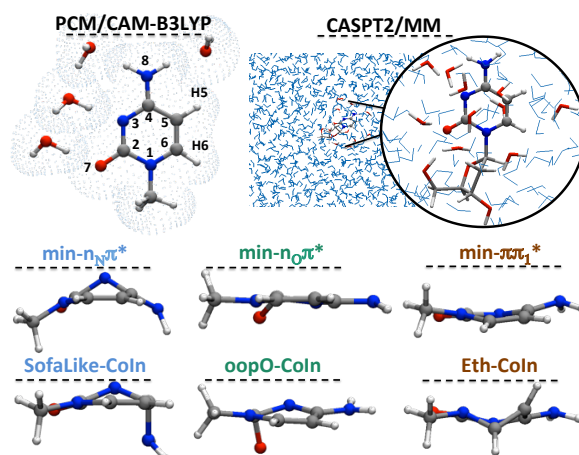


Figure 1. Representative schemes for cytosine molecule used in CAM-B3LYP PCM+4-H₂O (atom labeling is also shown) and CASPT2/MM calculations: low layer (LL) in sticks, the medium layer (ML) in tubes, and high layer (HL) in ball and sticks. Geometries of the most relevant stationary points of the dCyd excited state PES.

2. EXPERIMENTAL AND COMPUTATIONAL DETAILS.

Experimental Details: dCyd and 5mdCyd were purchased from Sigma-Aldrich and Fluorochem, respectively. Acetonitrile and tetrahydrofuran were obtained from Merck (UVA-sol grade). All chemicals were used without further purification. For the preparation of the aqueous solutions ultrapure water was used produced by a Milli-Q Synthesis system.

Absorption spectra were recorded with a Perkin Lambda 850 spectrophotometer. The fluorescence spectra were measured upon 267 nm excitation, with a Fluorolog-3 (Horiba, Jobin-Yvon) fluorimeter. For the fluorescence quantum yield measurements (Table 1), thymidine monophosphate (TMP) was used as reference ($\phi_{\text{fluo}} = 1.54 \times 10^{-4}$).⁵³

The femtosecond fluorescence upconversion apparatus has been described earlier.⁵⁴ The samples were excited at 267 nm which was generated as a third harmonic of a femtosecond mode-locked Ti-sapphire laser (Coherent MIRA 900). The average excitation power was set to 40 mW for dCyd and to 25 mW for 5mdCyd due to its higher photoreactivity. The

concentration of the solutions was varied between 10^{-4} and 10^{-3} mol·L $^{-1}$ and 25 to 50 mL solution was circulated in a flow system to avoid photodegradation which was especially important for 5mdCyd. The fluorescence decays were recorded between 330 and 380 nm. Parallel and perpendicular excitation/detection configurations were realized by controlling the polarization of the exciting beam with a zero-order half-wave plate, then the total fluorescence kinetics and the anisotropy decays were calculated.⁵⁵

The decays were analyzed following a non-linear fitting/deconvolution procedure using multi-exponential functions, $F(t) = \sum_{i=1}^2 a_i \exp(-t/\tau_i)$, convoluted with a Gaussian apparatus function. The fitting parameters as well as the average decay time, defined as $\langle \tau \rangle = \sum_{i=1}^2 a_i \tau_i / \sum_{i=1}^2 a_i$ where $\sum_{i=1}^2 a_i = 1$, are given on Table 2 (and S1-3).

Computational Details: TD-DFT. CAM-B3LYP and TD-CAM-B3LYP were used to characterize the ground and excited state minima of dCyd and 5mdCyd, using the 6-31G(d) basis set for geometry optimizations (TDCAM superscript), which was enlarged up to 6-311+G(d,p) for specific cases (see section 2.1 and Table S7 in SI). Polarizable Continuum Model (PCM)^{48,49} was used to simulate the different solvents and in the case of WAT, we included 4 explicit water molecules into the model (see Figure 1). All the calculations were performed with the Gaussian09 package.⁵⁶ After checking for dCyd in WAT that substitution of the sugar with a methyl group has a small effect on the excited state behavior (see Table S4), in order to decrease the computational cost, the remaining of our analysis was performed on 1-methyl-cytosine and 1,5-dimethyl-cytosine. However, since it is known that the presence of the sugar group can affect the photophysics of cytosine,²⁴ a detailed comparison between 1-methyl-cytosine and dCyd results can be found in section 3.1 of the SI.

CASPT2/MM. MM dynamics simulations (100 ns) were performed using the Amber-11⁵⁷ suite of programs and the FF99⁵⁸ force field for dCyd and 5mdCyd surrounded by a cubic box of TIP3P⁵⁹ water molecules. Cluster analysis (see section 2.2 in SI) provides the initial geometry for the QM/MM calculations (we have tested 4 different clusters). In this case a three-layer approach is used: the pyrimidine base considered at the QM level in the High Layer (HL), the sugar and the closest water molecules (5Å) into the mobile Medium Layer (ML), and the frozen Low Layer (LL) containing the rest of the solvent box. Both ML and LL were treated at the MM level. The QM part is coupled to the MM subsystem through electrostatic embedding, the point charges being considered in the QM computations as described elsewhere.⁶⁰ For the QM part the complete active space second-order perturbation theory (CASPT2)^{61,62} was used with an active space of 14 electrons in 10 orbitals (see Figure S3) selected (CASPT2 superscript). Further details on the state-average (SA), zeroth-order Hamiltonian and level shifts employed are given in the SI (Section 3.7 and Tables S6, S12-S35). The 6-31G(d) basis set was used for numerical CASPT2 gradients and geometry optimizations, whereas the larger ANO-L-VTZP basis was considered for refining the final CASPT2 energies. If not specified the multi state (MS) version of the CASPT2 method was considered (see SI for details).⁶³ The COBRAMM⁶⁴ interface was used for QM/MM energy and gradient calculations, combining Amber-11 (FF99⁵⁸ and TIP3P⁵⁹ force fields), MOLCAS8⁶⁵ (elec-

tronic structure CASPT2 calculations) and Gaussian09 (geometry optimization) packages.

All the computational analysis has been performed on the keto-amino tautomers, the most stable in all the solvents examined (see section 3.5 in the SI).

3. RESULTS

3.1.1. Steady State and Time Resolved Spectroscopic properties.

The absorption and fluorescence spectra of dCyd and 5mdCyd in the three solvents examined are shown in Figure 2 (and S1) and the spectroscopic parameters in Table 1 (and S1-2). The absorption spectrum of dCyd in WAT shows a maximum at 270 nm and a shoulder around 230 nm of similar intensity, hereafter labeled as band I and II, respectively. The absorption spectrum of 5mdCyd is similar to that of dCyd, but both bands I and II are red-shifted compared to dCyd.³¹ In the non-protic ACN and THF solvents, the absorption spectra are significantly red-shifted and the relative intensity of band II increases, appearing as a clear maximum (Figure 2a and 2c). In THF, for both dCyd and 5mdCyd, band II further shifts to longer wavelengths, without affecting the position of band I.

The fluorescence spectrum of 5mdCyd (Figure 2d) in non-protic solvents is red-shifted compared to WAT, as previously discussed.⁶⁶ For dCyd a similar red-shift is observed when going from WAT to THF (Figure 2b), but a significant (12 nm) blue-shift is found in ACN, accompanied by a 50 % increase of the fluorescence quantum yield (from 0.6×10^{-4} to 0.9×10^{-4}).

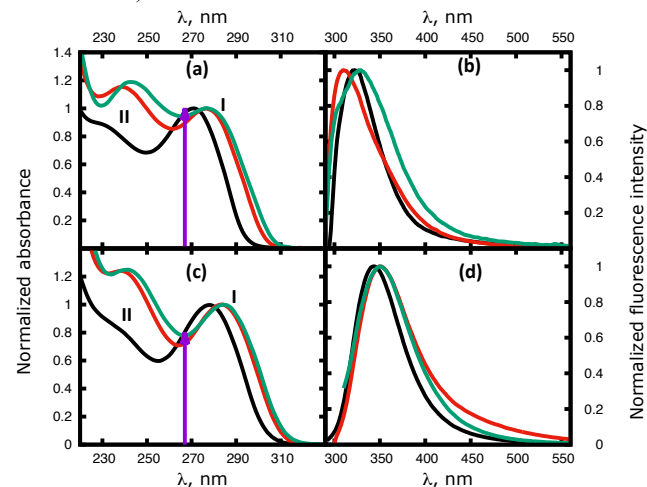


Figure 2. Steady-state absorption (a, c) and fluorescence (b, d) spectra of dCyd (top) and 5mdCyd (bottom) in WAT (black), ACN (red) and THF (green). The excitation wavelength (267 nm) of the fluorescence experiments is indicated by a purple arrow.

Table 1. Summary of the steady-state spectroscopic parameters of dCyd and 5mdCyd: λ_{max}^I and λ_{max}^{II} are the peak wavelengths of the

	dCyd				5mdCyd			
	Absorption		Fluorescence		Absorption		Fluorescence	
	λ_{max}^I	λ_{max}^{II}	$\lambda_{max}^{f_{two}}$	Φ_f	λ_{max}^I	λ_{max}^{II}	$\lambda_{max}^{f_{two}}$	Φ_f
WAT	271 (4.58)	230 (5.39)	323 (3.81)	0.6	278 (4.46)	242 (5.12)	344 (3.60)	6.4
ACN	277 (4.48)	239 (5.19)	311 (3.99)	0.9	283 (4.38)	238 (5.21)	352 (3.52)	4.9
THF	277 (4.48)	243 (5.10)	328 (3.78)	0.7	284 (4.37)	241 (5.15)	351 (3.53)	4.5

absorption of band I and band II respectively in nm (eV), λ_{max}^{fluo} is the peak wavelength of the fluorescence and ϕ_{fluo} is the fluorescence quantum yield $\times 10^{-4}$.

Table 2. Parameters derived from the fits of the fluorescence decays of dCyd at 330 nm and 5mdCyd at 350 nm with bi-exponential

	dCyd			
	τ_1 / ps	τ_2 / ps	$\langle\tau\rangle$ / ps	r_0
WAT	0.22±0.01 (49±4)	0.96±0.07 (51±4)	0.37±0.02	0.33±0.01
ACN	0.22±0.02 (22±3)	0.91±0.04 (78±3)	0.53±0.03	0.33±0.01
	5mdCyd			
	τ_1 / ps	τ_2 / ps	$\langle\tau\rangle$ / ps	r_0
WAT	1.25±0.04 (11±1)	8.0±0.1 (89±1)	^a 5.1±0.1	0.33±0.01
ACN	1.12±0.10 (8±1)	6.5±0.1 (92±1)	^b 4.7±0.1	0.26±0.01

functions, in water (WAT) and acetonitrile (ACN). τ_1 ($p_1\%$), τ_2 ($p_2\%$): time constants (and its corresponding weights). $\langle\tau\rangle$: average fluorescence lifetime. r_0 : initial anisotropy.

a) The average fluorescence lifetime at 380 nm are: a) 6.2±0.1 ps and b) 5.9±0.1 ps.

The fluorescence decays and anisotropies recorded at the fluorescence maximum, 330 and 350 nm, for dCyd and 5mdCyd, respectively, are shown in Figure 3. All fluorescence decays show non-exponential behavior and they were best fitted using a biexponential model (vide supra). The obtained parameters are shown in Table 2 and S3.

The time components of dCyd in WAT are about 0.2 (τ_1) and 1 ps (τ_2), with an average fluorescence lifetime ($\langle\tau\rangle$) of 0.37 ps at 330 nm; they do not show any significant dependence on the emission wavelength (see Table S3). In ACN the fluorescence decay is slower than in WAT (Figure 3a), being $\langle\tau\rangle$ 0.53 ps at 330 nm. The fluorescence decays of 5mdCyd are remarkably slower compared to dCyd both in WAT and ACN. Contrary to dCyd, the fluorescence decay of 5mdCyd is slightly slower in WAT than in ACN (see Figure 3c). The τ_1 and τ_2 decay times vary (depending on the emission wavelength) between 0.8 and 1.3 ps and 6.5 and 8.2 ps, respectively (see Table S3). The average fluorescence lifetime increases from ~3 to 6 ps with increasing emission wavelength in both solvents, following the same tendency described in water by Sharonov *et al.*³¹

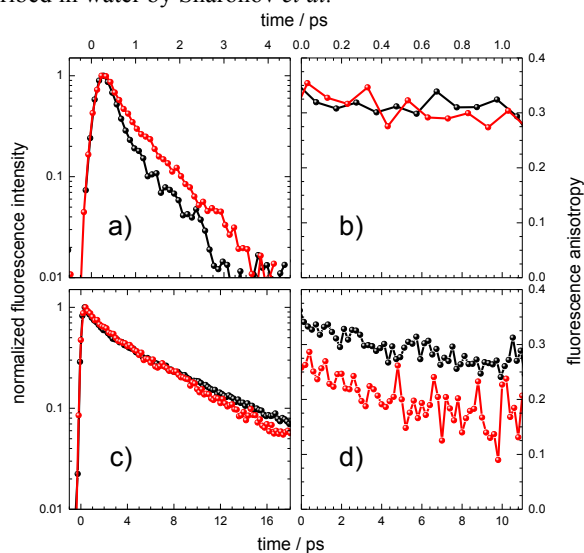


Figure 3. Time-resolved fluorescence decays (a, c) and fluorescence anisotropies (b, d) of dCyd (top; at 330 nm) and 5mdCyd

(bottom; at 350 nm) in WAT (black) and ACN (red). Excitation wavelength: 267 nm

The zero-time fluorescence anisotropy (r_0) of dCyd is rather high, ~0.33 in WAT and in ACN, in agreement with previous results in water and methanol.²⁴ The anisotropy does not show any noticeable dependence on the emission wavelength and it remains constant up to 1 ps: beyond this time, the anisotropy signals become too noisy to be determined.

The r_0 obtained for 5mdCyd depends on the proticity of the solvent, being much lower in ACN (0.26) than in WAT (0.33). The latter value is similar to that found in other protic solvents.²⁴

We highlight that while the steady-state spectroscopic parameters of dCyt and 5mdCyd are relatively strongly modulated when going from polar, protic solvent (water) to polar, non-protic solvents (ACN and THF), the fluorescence lifetime is not significantly affected. Interestingly, this effect contrasts with the behavior of uracil derivatives, namely thymine and 5-fluorouracil for which going from water to acetonitrile show a significant decrease of the bright state lifetime.³⁸

3.1.2. The excited states in the Franck-Condon region.

In Table 3 we report the Vertical Absorption Energies (VAEs) of the four (five in WAT) lowest energy excited states in the FC region, computed in the three solvents at the PCM/CAM-B3LYP/6-31G(d) level and in WAT at the MS-CASPT2/MM level (see also Table S5).

According to our calculations, for both dCyd and 5mdCyd, in all three solvents, 2 bright $\pi\pi^*$ transitions (the corresponding excited state will be denoted hereafter $\pi\pi_1^*$ and $\pi\pi_2^*$) can be associated to band I and band II, respectively. $\pi\pi_1^*$ derives from a HOMO→LUMO excitation (Figure S3), with a significant bonding/antibonding character for the C5=C6 double bond. For $\pi\pi_2^*$ the excitation involves HOMO-1 and LUMO orbitals. In agreement with the experimental spectra, our TD-CAM calculations predict that C5-methylation leads to a red-shift of $\pi\pi_1^*$ by 0.11 eV (0.27 eV at MS-CASPT2), whereas the remaining excited states are less affected. This effect can be explained by the larger antibonding contribution of methyl orbitals to the HOMO, decreasing the HOMO/LUMO gap (Figure S3).

From a quantitative point of view, MS-CASPT2/MM results (Table S6) are very close to the experimental absorption maximum of band I (overestimated by ~0.12 eV only), which would lead to a weak underestimation (~0.15 eV) once included vibrational and thermal effects (see below). PCM/TD-CAM-B3LYP/6-31G(d) VAE are instead blue-shifted by ~0.7 eV, and when using a more-extended basis set, by ~0.5 eV (Table S7). This residual error is mainly due to the lack of vibrational and thermal effects, whose inclusion would lead to an additional red-shift of the computed maximum, which would become very close to the experimental one (see the discussion in ref. ⁶⁶). In ref. ⁶⁶ we have already discussed how an increase of the solvent polarity and, especially, solute-solvent Hydrogen bonds explains the blue-shift of band I in WAT (see also SI). We here simply note that our calculations can reproduce the solvent effect also for dCyd, further supporting their reliability.

In ACN and THF, at the PCM/TD-CAM-B3LYP level, two dark excited states fall within these first four excited

states of dCyd. The excitations have a mixed character (the corresponding transition densities are shown in Figure S4); in the FC region, the lowest $n\pi^*$ (S_2) state mainly involves an excitation from the Lone Pair on the N_3 atom to the LUMO. We shall label this state as $n_N\pi^*$. S_4 receives contribution from excitation from the Lone Pair of the O_7 atom to the LUMO and LUMO+1. This state (labelled in the following as $n_O\pi^*$) is close in energy (0.08/0.09 eV) to $\pi\pi_2^*$ (S_3). C5-methylation does not qualitatively affect the shape of $n_N\pi^*$ and $n_O\pi^*$ states, but decreases their relative stability with respect to $\pi\pi_1^*$ by ~ 0.1 eV. In W9AT, both dark states are destabilized with respect to the $\pi\pi^*$ transitions and become strongly coupled with the higher bright excited states. S_2 and S_3 are then a mixture of the $n_N\pi^*$ and $\pi\pi_2^*$ diabatic states (see Figure S4). S_4 corresponds to another $\pi\pi^*$ transition (HOMO \rightarrow LUMO+1 excitation, $\pi\pi_3^*$) that is strongly stabilized in WAT, whereas $n_O\pi^*$ (where the weight of the $n_O\rightarrow$ LUMO+1 excitation increases) corresponds to S_5 . Increasing the basis set (Table S7) does not qualitatively change the description of the FC region. A strong coupling between the different excited states at the FC is confirmed by CASPT2/MM calculations (see Table S6) whose state ordering/energies (especially for the case of the $\pi\pi_2^*$ state) are dependent on the details of the computations (number of roots, basis set, SS/MS...etc, see Section 3.7 of the SI). The dependence on the QM/MM cluster used in the calculations is instead less significant (see SI). In Table 3 we report the MS-CASPT2/SA(8)CASSCF results, providing the same state ordering as the one described above for PCM/TD-CAM-B3LYP, since it has been used to compute the excited states' PES, though this level of calculations underestimates the absorption energy of $\pi\pi_2^*$. Further calculations providing less mixing between states and allowing, then, to obtain a more accurate estimate of its energy (see SI) placed the $\pi\pi_2^*$ state above in energy compared to the $n_N\pi^*$.

In agreement with what has been found for other pyrimidines,^{4,46} an increase of the solvent polarity and, especially, the presence of solute/solvent hydrogen bonds relatively destabilize $n\pi^*$ transitions of dCyd with respect to $\pi\pi^*$ transitions.⁴⁷

On the ground of the data just reported, it is easier to appreciate some of the peculiarities of dCyd and to understand which the most debated issues are (see SI section 3.6 for a more detailed discussion). First of all, band II (associated to $\pi\pi_2^*$) is rather close in energy to band I and, especially in ACN and THF, more intense. Excitation at 267 nm (Figure 2) brings an important part of the population to $\pi\pi_2^*$. Furthermore, the absorption spectrum is very broad, with a significant overlap between band I and II. Considering that at least two dark excited states fall very close to 267 nm, a significant vibronic coupling between the different bands is expected. It is thus clear that a complete study of dCyd photophysics requires that the interplay between all the five lowest energy states (*i.e.* S_0 , $\pi\pi_1^*$, $\pi\pi_2^*$, $n_N\pi^*$ and $n_O\pi^*$) is considered. This obviously increases the number of possible deactivation routes (see the next section), and explains why, for instance, the main CoIn for the non-radiative decay of the bright excited states has not been assessed so far. The reasons for the experimental bi-exponential fluorescence decay have also been discussed; according to a recent proposal the fastest component is associated to a part of the photoexcited state population decaying directly from the FC region to S_0 ,²⁴ whereas the longer component passes through a minimum on $\pi\pi_1^*$.

The involvement of dark states along the decay mechanism of dCyd is another major point of debate, being the focus of many theoretical studies.^{11,13,14,16,39,44} Although the most recent contributions agree in assigning the long excited state lifetime (from tens to hundreds of ps) to a dark singlet state, the nature (*i.e.* $n_N\pi^*$ or $n_O\pi^*$) of this state remains elusive.²⁰⁻²⁷

Finally, it is important to understand why excited-state decay is slower in 5mdCyd and no significant involvement of dark $n\pi^*$ state is found (see below), as discussed in a very interesting and thorough recent experimental study.²⁴

Table 3. Vertical absorption energy (in eV) and oscillator strength (in parentheses) of the four lowest excited states computed at the PCM/TD-CAM-B3LYP or at the MS-CASPT2/MM level.

	dCyd			
	THF/CAM-B3LYP	ACN/CAM-B3LYP	WAT/CAM-B3LYP+ 4 H ₂ O	WAT/MS-CASPT2/MM
$\pi\pi_1^*$	5.12 (0.14)	5.15 (0.14)	5.27 (0.21)	4.46 (0.07)
$n_N\pi^*$	5.64 (0.00)	5.70 (0.00)	^a 6.10 (0.09)	^c 5.65 (0.02)
$\pi\pi_2^*$	6.08 (0.22)	6.11 (0.22)	^a 6.00 (0.09)	^c 4.79(0.15)
$n_O\pi^*$	6.16 (0.00)	6.20 (0.00)	^b 6.61 (0.00)	^d 5.98 (0.00)
	5mdCyd			
	THF/CAM-B3LYP	ACN/CAM-B3LYP	WAT/CAM-B3LYP+ 4 H ₂ O	WAT/MS-CASPT2/MM
$\pi\pi_1^*$	5.02 (0.14)	5.04 (0.14)	5.16 (0.20)	4.19 (0.07)
$n_N\pi^*$	5.61 (0.00)	5.66 (0.00)	^a 5.96 (0.07)	^a 5.55 (0.01)
$\pi\pi_2^*$	6.09 (0.18)	6.11 (0.18)	^a 6.08 (0.11)	^a 4.79 (0.07)
$n_O\pi^*$	6.14 (0.00)	6.19 (0.00)	^c 6.64 (0.00)	^f 5.77 (0.00)

a) Strong mixing between $\pi\pi_2^*$ and $n_N\pi^*$; b) S_5 , with strong mixing to LUMO and LUMO+1 excitation. S_4 (6.55 eV, 0.18) in this case corresponds to $\pi\pi_3^*$ transition HOMO \rightarrow LUMO+1; c) S_5 , with strong mixing to LUMO and LUMO+1 excitation. S_4 (6.48 eV, 0.28) in this case corresponds to $\pi\pi_3^*$ transition HOMO \rightarrow LUMO+1 d) S_5 , with strong mixing to LUMO and LUMO+1 excitation. S_4 (5.41 eV, 0.08) in this case corresponds to $\pi\pi_3^*$ transition HOMO \rightarrow LUMO+1 e) not mixed at the MS-CASPT2 level of theory but strongly mixed at the SS-level (see Table S6) f) S_4 (5.59 eV, 0.) in this case corresponds to $\pi\pi_3^*$ transition HOMO \rightarrow LUMO+1.

3.2 The decay of Bright Excited States of dCyd

3.2.1 The lowest energy bright excited state: $\pi\pi_1^*$

For dCyd both PCM/TD-CAM-B3LYP and CASPT2/MM calculations predict that a steep path leads the $\pi\pi_1^*$ state from the FC region to a pseudo minimum (the energy gradient $\sim 4\times 10^{-4}$ a.u., see Figure 4a) min- $\pi\pi_1^*$ -pla, where the pyrimidine ring remains almost planar and the main geometry shifts concern the C_5C_6 bond (see Figure 1), in line with the bonding/antibonding nature of the MO's involved in the transition).^{11,16,42-44}

Vertical Emission Energy (VEE) from the 'planar' region would fall at 3.58 eV (~ 346 nm) at the CASPT2/MM level, nicely matching observations, and at 4.57 eV at the PCM/TD-CAM-B3LYP level. In the following we abbreviate the level of theory as TDCAM for the PCM/TD-CAM-B3LYP/6-31G(d) and CASPT2 for the MS-CASPT2(14,10)/ANO-L/MM calculations. As discussed above, at TDCAM level (without considering vibronic and thermal effects) the VAE is significantly blue-shifted with respect to experiments. Our analysis is therefore mainly based on the comparison between the computed Stokes shift

with the difference between the experimental absorption and fluorescence maxima. The computed Stokes shift at $\min-\pi\pi_1^*$ -pla is $^{\text{TDCAM}}0.70$ eV and $^{\text{CASPT2}}0.88$ eV, both consistent with an experimental Stokes shift of 0.76 eV. $\min-\pi\pi_1^*$ -pla is not the global minimum, which instead ($\min-\pi\pi_1^*$ in Figure 4a) presents a ‘bent’ pyrimidine ring (Figure 1). However, $\min-\pi\pi_1^*$ is almost degenerate with $\min-\pi\pi_1^*$ -pla, but the VEE is significantly smaller (by ~ 0.6 - 0.8 eV both at the TDCAM and CASPT2 levels); as a consequence the computed Stokes shift at $\min-\pi\pi_1^*$ are significantly larger ($^{\text{TDCAM}}1.47$ eV and $^{\text{CASPT2}}1.45$ eV). The path from the FC region to both minima, $\min-\pi\pi_1^*$ -pla/ $\min-\pi\pi_1^*$, does not significantly affect fluorescence anisotropy ($^{\text{TDCAM}}0.394/0.399$ and $^{\text{CASPT2}}0.386/0.380$ for $\min-\pi\pi_1^*$ -pla/ $\min-\pi\pi_1^*$, respectively). Please note that the CASPT2/MM picture does not depend on the cluster used as starting point in the geometry optimizations.

We have then explored how these minima could further deactivate towards the S_0 . In analogy with the results obtained in the GP,^{6,11,13,14} we located a crossing region with S_0 , the well-known ethene-like conical intersection (Eth-CoIn, Figure 1), characterized by the out-of-plane deviation of the C_5 - C_6 bond substituents. Eth-CoIn is more stable than $\min-\pi\pi_1^*$ by ~ 0.2 eV at the TDCAM and CASPT2 levels. (Figure 4a) Furthermore, TDCAM Linear Interpolation Cartesian Coordinates (LICC) (see SI) indicate that this crossing region is separated from $\min-\pi\pi_1^*$ by a vanishingly small energy barrier (< 0.1 eV), considering that this procedure provides upper limits of the ‘real’ energy barrier. The energy barrier between $\min-\pi\pi_1^*$ and the Eth funnel is slightly larger (0.18 eV) according to the optimized CASPT2 transition state (TS).

The picture provided by our calculations is fully consistent with the experimental fluorescence spectra. A large plateau, giving account of the broad steady-state spectrum, separated by a very small (or zero) energy barrier from an effective CoIn, explains the sub-ps excited state lifetime.

The global decay picture is almost unaffected by changing the solvent from WAT to ACN and THF. PCM/TDCAM calculations in ACN and THF also locate both planar (4.74 and 4.70 eV) and non-planar minima (4.73 and 4.69 eV) and connect them to the Eth funnel (4.57 and 4.46 eV) without any significant energy barrier.

3.2.2. The second bright excited state $\pi\pi_2^*$

In WAT, TDCAM predicts that optimization of the $\pi\pi_2^*$ state leads barrierless to a crossing with $\pi\pi_1^*$ (after crossing $n_N\pi^*$) followed by subsequent decay to the $\pi\pi_1^*$ minimum. Interestingly, close to the energy of the $\pi\pi_2^*$ state at the FC region (6.00), a crossing between $\pi\pi_2^*/n_O\pi$ states is located (~ 6.30 eV). The first part of the mechanisms is similar at the CASPT2. The $\pi\pi_2^*$ state crosses the $n_N\pi^*$ state (at the level of theory used in the $^{\text{CASPT2}}$ optimization at FC $n_N\pi^*$ is more stable than $\pi\pi_2^*$), and then reaches the $\pi\pi_2^*/\pi\pi_1^*$ funnel. From there two paths are accessible: i) one leads to the $\min-\pi\pi_1^*$ and ii) another one populating a local minimum on the $\pi\pi_1^*$ PES, $\min-\pi\pi_1^*$ -2 at 4.23 eV, less stable than $\min-\pi\pi_1^*$ -pla and $\min-\pi\pi_1^*$. This new minimum, where the $\pi\pi_1^*$ is more strongly coupled with the $n_O\pi^*$ state, is connected to the S_0 through a different CoIn, the so-called semi-planar-CoIn funnel (4.80 eV), described below in detail. Its emis-

sion energy is 3.68 eV, which gives a Stokes shift of 0.78 eV.

Absorption to $\pi\pi_2^*$ followed from emission from the $\min-\pi\pi_1^*$ -pla is associated to a negative fluorescence anisotropy: -0.02 and -0.18 according to TDCAM and CASPT2, respectively.

TDCAM in ACN and THF provides a behavior similar to that found in WAT, with a very steep path leading $\pi\pi_2^*$ to a crossing with $\pi\pi_1^*$, followed to decay to $\min-\pi\pi_1^*$.

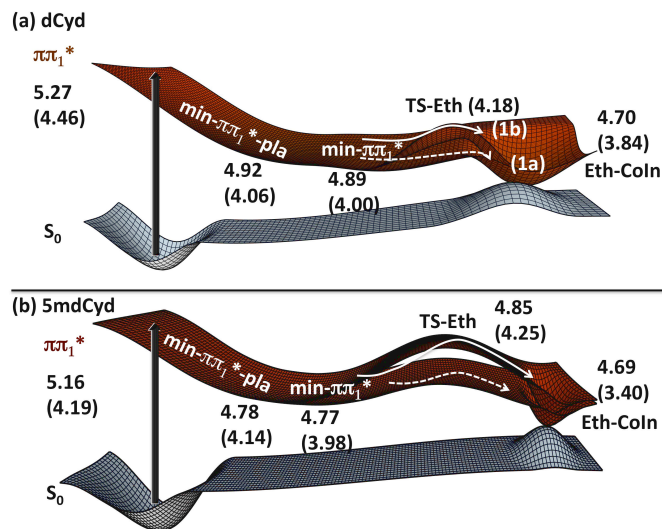


Figure 4. Main deactivation pathways along the $\pi\pi_1^*$ for dCyd (a) and 5mdCyd (b) predicted by TD-CAM-B3LYP/6-31G(d) calculations in water (dashed lines) and QM (MS-CASPT2(14,10)/ANO-L)/MM calculations (energies in parenthesis and solid lines). Energies relative to the S_0 (in eV).

3.3 The decay of dark Excited States of dCyd

Independently of the adopted computational method, in WAT $n_N\pi^*$ (in the FC region $^{\text{TDCAM}}6.10$; $^{\text{CASPT2}}5.65$ eV) is predicted to decay towards its minimum ($\min-n_N\pi^*$) in the S_1 PES (see Figure 5a), after crossing $\pi\pi_1^*$. This crossing (whose absolute energy is $\sim ^{\text{TDCAM}}5.61/^{\text{CASPT2}}4.72$ eV) is characterized by the lengthening of the N_3 - C_4 and N_1 - C_6 bonds by 0.03-0.04 Å. In $\min-n_N\pi^*$, in addition to a further increase of these bond lengths, N_3 atom (also C_2 and C_4 to a lesser extent) significantly moves out of the molecular plane (see Figure 1). At the TDCAM $\min-n_N\pi^*$ and $\min-\pi\pi_1^*$ are almost degenerate, whereas according CASPT2/MM $\min-n_N\pi^*$ is ~ 0.5 eV less stable than $\min-\pi\pi_1^*$.

The closest crossing region with S_0 for $\min-n_N\pi^*$ is the so-called SofaLike-CoIn, see Figure 1, which still shows its typical N_3 out of plane but slightly recovers the planarity of the rest of the cycle. According to both TDCAM and CASPT2 the SofaLike-CoIn is significantly higher in energy (~ 0.60 eV) than $\min-n_N\pi^*$ (Figure 5a).

LICC calculations (see Table S9) provide a barrier of $^{\text{TDCAM}}0.47$ eV and $^{\text{CASPT2}}0.34$ eV on the path connecting $\min-n_N\pi^*$ and $\min-\pi\pi_1^*$, decreasing to $^{\text{TDCAM}}0.36$ eV upon location of the TS (AE $^{\text{TDCAM}}5.19$ eV).

Geometry optimizations of $n_O\pi^*$ leads to a minimum, $\min-n_O\pi^*$ (also corresponding to a S_1 minimum), after crossing all the lower-lying excited states (see SI). $\min-n_O\pi^*$ is characterized by the lengthening of the C-O bond and by an out

of plane distortion of the carbonyl group (Figure 1, the dihedral angle $dO_7C_2N_3N_1$ -131°).

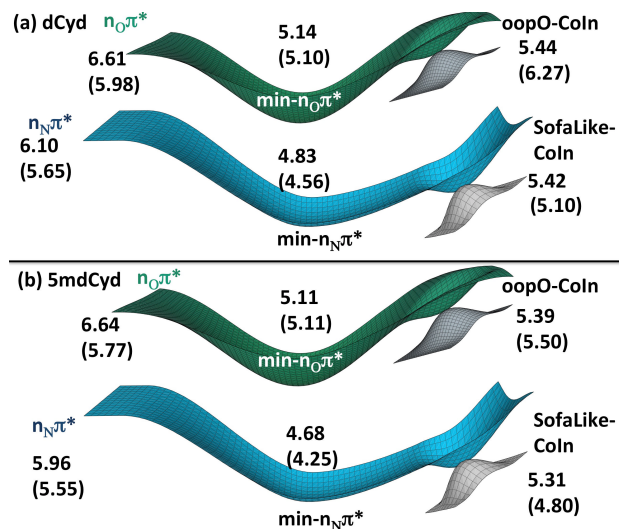


Figure 5. Main deactivation pathways along the dark states ($n_N\pi^*$ and $n_O\pi^*$) for dCyd (a) and 5mdCyd (b) predicted by TD-CAM-B3LYP/6-31G(d) calculations in water and QM (MS-CASPT2(14,10)/ANO-L)/MM calculations (energies in parenthesis). Energies and relative to the S_0 (in eV).

The structure of $min-n_O\pi^*$ does not depend on the cluster used in the CASPT2/MM optimizations, whereas its adiabatic stabilization with respect to the FC point exhibits a more significant dependence (0.9–1.5 eV) on the water arrangement (see table S39 in the SI).

According to TDCAM, a crossing region with S_0 can be reached from $min-n_O\pi^*$ (Figure 5a) after further distorting the dihedral ($dO_7C_2N_3N_1$ to -105°) (oopO-CoIn in Figure 1), 0.3 eV less stable than $min-n_O\pi^*$. At the CASPT2 level this funnel seems inaccessible (1.2 eV higher than $min-n_O\pi^*$). According to CASPT2, another CoIn is instead more easily accessible, the semi-planar three-state CoIn (4.80 eV), which can be reached after overpassing a 0.5 eV TS. This CoIn (already discussed in GP studies on cytosine)^{15,67} connect $\pi\pi_1^*$, $n_O\pi^*$ and S_0 ; the pyrimidine ring has a semi-planar arrangement, with the H_6 atom out of the molecular plane, but its main characteristic is a significantly elongated C-O bond (1.65 Å). The semi-planar-CoIn at the TDCAM level is instead hugely destabilized, being more than 1 eV higher in energy than $min-n_O\pi^*$.

LICC calculations on the path connecting $min-n_O\pi^*$ and $min-\pi\pi_1^*$ suggests a substantial energy barrier ($TDCAM^{0.50}$ eV and $CASPT2^{0.27}$ eV), decreasing again to $TDCAM^{0.20}$ upon location of the TS ($TDCAM^{5.31}$ eV).

TDCAM calculations in ACN and THF show that the decay mechanism is not qualitatively affected by the solvent (see SI). The energy barriers from the minima towards the crossing region with S_0 are also similar. The most significant differences with respect to WAT concern the path connecting the dark and bright excited state minima. In ACN and THF the energy barrier in the path connecting $min-\pi\pi_1^*$ and

$min-n_N\pi^*$ is much lower than in WAT (0.08 eV vs 0.36 eV). Analogously, the LICC $min-n_O\pi^*/min-\pi\pi_1^*$ provides a much smaller energy barrier (0.10 eV in ACN/THF vs 0.50 eV in WAT), making impossible to optimize the TS.

3.4 C5-methylation: Bright and Dark Excited States of 5mdCyd.

In 5mdCyd we obtain for $\pi\pi_1^*$ and $\pi\pi_2^*$ (see SI) a qualitatively similar picture (Figure 4b) to that depicted above for dCyd, but with two significant quantitative differences. A steep path on $\pi\pi_1^*$ leads to a pseudo-planar minimum and to a ‘bent’ minimum. For 5mdCyd, however, the absolute minimum is close to be planar (the deviation from planarity is only ~10°), and, consequently the computed Stokes shift in the two structures is similar ($TDCAM^{0.81}$ and $TDCAM^{0.96}$ eV; $CASPT2^{0.89}$ and $CASPT2^{0.95}$ eV) to the experimental value at 0.84 eV. The most accessible CoIn (Eth-CoIn) is similar to that found for dCyd, but in this case a larger energy barrier (TS) separates the crossing region from $min-\pi\pi_1^*$, $TDCAM^{0.08}$ eV and $CASPT2^{0.3}$ eV. The C5-methyl moiety, due to its electronic interaction with C_5C_6 double bond, increases the tendency of the pyrimidine ring to remain planar, and, consequently, the energetic cost for out-of-plane distortion of the C_5 group. The global decay picture is almost unaffected in ACN and in THF; in these two latter solvents $min-\pi\pi_1^*$ and the Eth-CoIn funnel are separated by an energy barrier of $TDCAM^{0.07}$ eV.

Our calculations predict that $\pi\pi_2^*$ decays to $\pi\pi_1^*$ in all the solvents.

C5-methylation does not significantly affect the decay paths of $n_N\pi^*$ and $n_O\pi^*$ (Figure 5b and SI). The only significant difference concerns the most easily accessible CoIn from $min-n_O\pi^*$ according to CASPT2, which is now the oopO-CoIn (Figure 1), in agreement with the TDCAM predictions. The two methods provide also a similar estimate of the energy necessary to reach this funnel from $min-n_O\pi^*$ ($CASPT2^{0.4}$ eV and $TDCAM^{0.3}$ eV).

3.5 Time Resolved Spectroscopic Properties: TIR and TA spectra of dCyd and 5mdCyd.

Looking for a general mechanistic model for the excited state decay of dCyd and 5mdCyd, as a next step of our analysis we have simulated the transient IR (TIR) and the Transient absorption (TA) spectra relative to the different stationary and pseudo-stationary points of the PES. Experimental TIR spectra show the signature of a long-living excited state (30–40 ps), traditionally attributed to one of the two dark states, $n_N\pi^*$ or $n_O\pi^*$.^{22,23} The difference IR spectra computed by TDCAM in WAT for $min-n_N\pi^*$ and $min-n_O\pi^*$ present very similar negative features (corresponding to the ground state bleaching) but the positions of the positive marker bands (due to the excited state vibrational modes) are different. For $n_N\pi^*$ we find two peaks at 1641 cm^{-1} and 1542 cm^{-1} , whereas a single strong positive peak at 1572 cm^{-1} is found for $n_O\pi^*$, assigned to in-phase stretching of C_2O_7 , C_5C_6 and C_4N_3 bonds. As shown in Figure 6, the TIR spectra computed for $n_O\pi^*$ is extremely close to the experimental spectrum of dCyd extracted from ref. 23.

TA experiments have been interpreted in the framework of two different time-regimes.²⁴ On a <4 ps time-scale, the

spectra are dominated by a negative peak at 350 nm, due to stimulated emission, and two positive features, at 300 nm and a broad one between 400-500 nm. As shown in Figure 6a, the CASPT2 computed excited state absorption (ESA) for $\text{min-}\pi\pi_1^*$ and $\text{min-}\pi\pi_1^*\text{-pla}$ is fully consistent with the experimental spectrum (the stimulated emission is not considered at this stage). Concerning the long-living features, displayed on the same time-scale of the state responsible of the TIR spectra, a weak positive signal, decreasing when going from 300 nm towards 600 nm is found. The computed CASPT2 ESA for $n_o\pi^*$ is consistent with the experimental one, whereas that obtained for $n_N\pi^*$ is too weak and does not exhibit any maximum at ~ 300 nm.

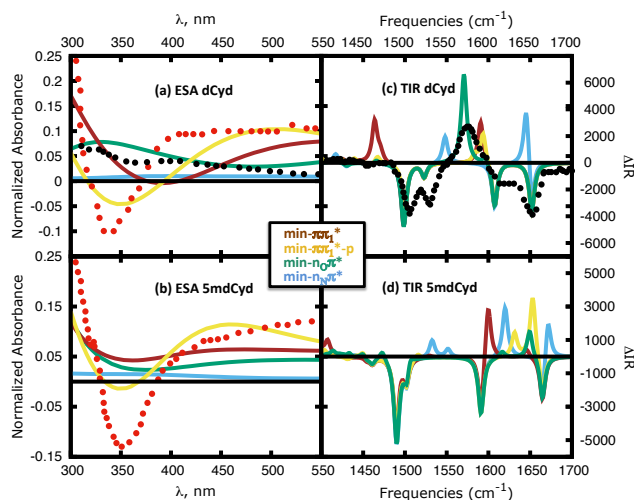


Figure 6. CASPT2/MM calculated excited state absorption spectra (at the MS-CASPT2 optimized geometries for the different stationary points) for dCyd (a) and 5mdCyd (b) and TDCAM transient infrared spectra (at the TDCAM optimized geometries) for dCyd (c) and 5mdCyd (d). See the central panel for color code. In dots, experimental TA and TIR spectra (excitation at 267 nm) extracted from Ref ²⁴ and Ref ²³, respectively.

The same kind of spectra for 5mdCyd can be found in Figure 6b and d being similar to the ones computed for dCyd. Our CASPT2 ESA present absorptions at ~ 450 nm in agreement with the experimental one,²⁴ corresponding to both the $\text{min-}\pi\pi_1^*$ and $\text{min-}\pi\pi_1^*\text{-pla}$. TDCAM TIR spectra for the dark excited states $n_N\pi^*$ is also similar to the one computed for dCyd. In this case, the $n_o\pi^*$ TIR does not present a significant signature at ~ 1550 cm^{-1} , since the correspondent stretching mode intensity is very weak. Unfortunately, there is no experimental TIR data for this compound to compare with.

4. DISCUSSION

As reported in Section 3.1, several basic questions concerning the excited state decay of dCyd and 5mdCyd in solution were still unanswered. They can provide a useful framework for discussing the main results of our joint experimental and computational study.

What is the path responsible of the sub-ps features in dCyd? Our calculations show that, for all solvents examined, an almost barrierless path on $\pi\pi_1^*$ connects the FC region to a CoIn (Eth-CoIn) with S_0 . On the other hand, while the first part of the PES, leading to a planar plateau, is steep, the latter portion is rather flat and another shallow

minimum is present. This picture is consistent with (and explains) the experimental fluorescence results, that are i) an ultrafast decay (0.40-0.70 ps), ii) very low fluorescence quantum yield ($\sim 10^{-5}$) and iii) a very broad fluorescence spectrum. Computed ESA spectra at the $\pi\pi_1^*$ minima are also consistent with the corresponding experimental signals,²⁴ confirming its population. Concluding, the $\pi\pi_1^*$ state (and the Eth-CoIn funnel) is driving the fastest decay of the fluorescence in all examined solvents, whereas the other states and CoIns documented here (e.g., the Sofa-like CI) are not significantly involved in these deactivations.

What is the role of the higher lying bright excited states? In agreement with the experimental absorption spectra, both computational methods predict that, following 267 nm excitation, the $\pi\pi_2^*$ state, close in energy (further details on the energy gap at the CASPT2 level are given in the SI) to the lower lying $\pi\pi_1^*$ state and with significant oscillator strength, is populated. In order to explore the effect of thermal fluctuations in the FC region, a MD dynamics has been run (see section 3.3 in the SI) and subsequently we have analyzed both the mixing between the $\pi\pi_1^*$ and $\pi\pi_2^*$ spectroscopic states and the overlap of the two absorption bands in the spectra. The results show that $\pi\pi_2^*$ is significantly mixed with $\pi\pi_1^*$ (averaged weight ~ 0.1 Figure S6) and that the excitation wavelength 267 also covers part of the second absorption band (see Figure S5). Then, *a priori* this state can be populated either at FC or at its vicinity. However, TDCAM does not suggest any significant role of the $\pi\pi_2^*$ population in the photoactivated dynamics in all solvents examined for times longer than 100 fs; there is no minimum on $\pi\pi_2^*$, whereas a steep path (suggesting a very effective ultrafast decay) leads to a crossing with $\pi\pi_1^*$, the system then following the same route described above. Actually, assuming a very fast $\pi\pi_2^* \rightarrow \pi\pi_1^*$ decay would provide zero-time fluorescence anisotropies fully consistent with the experimental results. CASPT2 also suggests a fast $\pi\pi_2^* \rightarrow \pi\pi_1^*$ decay, thus confirming $\pi\pi_1^*$ as the main route for the ultrafast decay in dCyd. A different $\pi\pi_1^*$ minimum ($\text{min-}\pi\pi_1^*\text{-2}$) can be populated though. According to our calculations, $\text{Min-}\pi\pi_1^*\text{-2}$ does not play a significant role in the fastest decay in dCyd, since it is separated by an energy barrier of 0.6 eV from the closest CoIn. On the other hand, its presence could affect the $\pi\pi_2^* \rightarrow \pi\pi_1^*$ decay, contributing to the multi-exponential fluorescence decay observed and, in particular, to the slower ultrafast decay component observed in dCyd (τ_2 , Table 2). $\text{Min-}\pi\pi_1^*\text{-2}$ could also act as ‘doorway’ to $n_o\pi^*$, since it is characterized by a longer CO distance. In general, as discussed below, our calculation suggests that $\pi\pi_2^*$ is the main responsible of the population of $n_o\pi^*$, not only because gives access to $\text{Min-}\pi\pi_1^*\text{-2}$, but also for the presence of $\pi\pi_2^*/n_o\pi^*$ in the vicinity of the FC region.

What is the role of the dark excited states? The two lowest energy dark excited states, $n_N\pi^*$ and $n_o\pi^*$, are placed at FC (in WAT) almost 1 eV higher than $\pi\pi_1^*$. However, the dark states are significantly mixed with all the bright excited states ($\pi\pi_1^*$, $\pi\pi_2^*$, $\pi\pi_3^*$) in this region, according to both TDCAM and CASPT2, enabling their population. A preliminary analysis based on CASSCF wavefunction coefficient of the different excitations suggests a strong mixing, also close to the FC region, for what concerns especially $n_o\pi^*$ and $\pi\pi_2^*$ states. These two states exhibit the largest mixing for all the structures sampled by the MD dynamics (0.4, Figure S6).

Actually, TA and TIR experiments show the presence of a long-living state, decaying on a 30–40 ps time scale, which is not observed by FU and points out to be a dark state. Our ESA and TIR calculations allow unambiguously assigning this state to $n_{\text{O}}\pi^*$. Although in the FC region $n_{\text{O}}\pi^*$ is less stable than the spectroscopic states, the analysis of the wavefunction coefficients shows that $n_{\text{O}}\pi^*$ is much more mixed with the bright states compared to $n_{\text{N}}\pi^*$ (coefficients 3–4 times larger), and, therefore, much more likely to be populated. A purposely tailored quantum dynamical study in solution could provide definitive insights on the effects responsible for $n_{\text{O}}\pi^*$ population. In this respect it is noteworthy that semiclassical dynamical studies in the gas phase have shown that the $n_{\text{O}}\pi^*$ is populated along a non-negligible percentage of trajectories¹⁸ despite being also higher in energy than the $\pi\pi^*$ state at the FC region. Furthermore, at difference of $\text{min-}n_{\text{N}}\pi^*$, $\text{min-}n_{\text{O}}\pi^*$ is separated by sizeable energy barriers from the other excited states. PCM/TD-CAMB3LYP calculations also show that, once $n_{\text{O}}\pi^*$ is populated, solvent degrees of freedom strongly stabilizes its minimum, characterized by a significant lengthening of the carbonyl bond-length, suggesting a partial dipolar character of the single bond (C^+-O^-), increasing its lifetime. This is further confirmed by additional QM/MM CASPT2 computations with different water arrangements (see SI section 3.7), confirming that a proper treatment of $n_{\text{O}}\pi^*$ requires the explicit inclusion of the water molecules hydrogen-bonded to the carbonyl group.

For the other solvents, unfortunately no TIR experiments are available. Our calculations show that dark states are relatively stabilized with respect to WAT, but, at the same time, the energy barrier separating the minima from the $\pi\pi_1^*$ funnel are very small. Thus, even if populated with an appreciable yield in the FC region, in ACN they could rapidly decay to $\pi\pi_1^*$, without giving rise to any long living features. At the same time, this repopulation could modify the shape of the S_1 PES, increasing the size of the region that the WavePacket (WP) on $\pi\pi_1^*$ can explore, leading to a small slowing down of the decay (see below).

What is the effect of methylation? In all solvents examined experiments show that C5-methylation leads to a ~6-fold increase of the excited state average lifetime (from 0.4–0.7 ps to 3.6–6.2 ps). Our calculations explain this effect with a larger energy barrier on the $\pi\pi_1^*$ path towards the ground state, present in all investigated solvents. This reasoning is based on static computations and it highlights the effect that methylation has on the excited state PESs of Cyd. Kinetic effects that could also play a role in the decay mechanism are not discussed here. Previous experiments²⁴ show that no signature of dark state population is found for 5mdCyd. Our calculations show that C5-methylation does not significantly affect the decay paths of the dark state. However, 5mdCyd dark states are destabilized in the FC region with respect to all the bright excited states, making them less likely to be populated. By inspecting Figure S6, it can be seen that no significant mixing is observed between any bright $\pi\pi^*$ and dark $n\pi^*$ states, in contrast to dCyd.

What are the main difference between the excited state decay of dCyd in the gas phase and in water?

TR experiments for C in the gas phase find multi-exponential decay, with one constant < 100fs, one constant ~1 ps and, according to some studies, a third time constant (3ps or 55 ps).^{68–70} This is a very different picture with respect to that documented here and by Kwok and co-workers²⁴ in WAT. Without entering in the interpretation of the gas phase experiments,⁴ our calculations show that solvent is expected to strongly affect photoactivated dynamics.

A first point to remind is that, as opposed to gas phase, in water the keto-amino tautomer is the most stable. For what concerns the excited states, the dark $n_{\text{N}}\pi^*$ state is radically different and is largely destabilized by solvent. For instance, the SofaLike-CoIn is ^{CASPT2}1eV higher in energy with respect to the $\text{min-}\pi\pi_1^*$ in WAT, whereas previous work reported values significantly lower 0.2–0.5 eV for this barrier in gas phase.^{11,14,45,71} A much larger barrier also separates the $n_{\text{N}}\pi^*$ and $\pi\pi_1^*$ minima.

The changes found in the $n_{\text{N}}\pi^*$ PES affects also the path leading from $\text{min-}\pi\pi_1^*$ to Eth-CoIn, although the barrier (^{CASPT2}0.15 eV) is similar to that obtained in the gas phase for cytosine at the MS-CASPT2 level (~0.1 eV).^{11,14,45,71} In the gas phase an interplay between $n_{\text{N}}\pi^*$ and $\pi\pi_1^*$ is possible and the PES of the S_1 adiabatic state is flatter than in water.^{11,13}

Also for the other dark state, $n_{\text{O}}\pi^*$, the barrier to access the semiplanar-CoIn is much larger in WAT (0.5 eV) than in gas phase (0.2 eV) according to CASPT2 calculations.¹⁴

What is the effect of the different solvents on the excited state decay? Our calculations show that the decay path on $\pi\pi_1^*$ is not significantly affected by the solvent; both for dCyd and 5mdCyd the energy barrier separating $\text{min-}\pi\pi_1^*$ from Eth-CoIn has a similar value in all the three solvents examined. Time Resolved experiments provide a similar conclusion, since both in WAT and in ACN the fluorescence decays on the sub-ps scale for dCyd and on ~5 ps scale for 5mdCyd. The only significant feature evidenced by FU experiments is a small ‘slowing-down’ of the dCyd decay in ACN, mirrored by a larger fluorescence quantum yield. According to our calculations, this result can be explained by a small involvement of $n_{\text{N}}\pi^*$ in the ultrafast dynamics. In ACN, $n_{\text{N}}\pi^*$ is indeed much closer to $\pi\pi_1^*$ in the FC region, increasing the possibility of its population, followed by decay to $\text{min-}n_{\text{N}}\pi^*$. However, in WAT, $\text{min-}n_{\text{N}}\pi^*$ is destabilized and substantial energy barrier separates $\text{min-}n_{\text{N}}\pi^*$ from the crossing with S_0 (0.6 eV) and with $\pi\pi_1^*$ (0.3 eV). Contrary, in ACN $\text{min-}n_{\text{N}}\pi^*$ and $\text{min-}\pi\pi_1^*$ are instead separated by a much smaller barrier (<0.1 eV); we are in the presence of a flat S_1 PES (see SI), where the WP can be spread, before decaying through Eth-CoIn, in line with a slightly longer lifetime. Solvent has a somewhat similar effect also for $n_{\text{O}}\pi^*$; in WAT, the energy barrier separating $\text{min-}n_{\text{O}}\pi^*$ and $\text{min-}\pi\pi_1^*$ (0.20 eV) is significantly larger than in non-protic solvents (LICC providing barriers <0.1 eV), mainly thanks to the stabilization of $\text{min-}n_{\text{O}}\pi^*$. Solvent can affect at different levels the excited state dynamics, and the final outcome cannot be predicted only by analyzing a single particular feature (e.g. the relative stability of the excited states in the FC region). It is now well known that hydrogen-bonding (HB) solvents decrease the stability of the $n\pi^*$ states involving a carbonyl lone-pair in the FC region.⁴ On the other hand, we here show that the lengthening of the CO bond, the most significant structural shift found in $\text{min-}n_{\text{O}}\pi^*$ is favored by solute-solvent hydrogen bonds. Since the main doorway

for $n_o\pi^*$ population is $\pi\pi_2^*$, $n_o\pi^*$ can be populated also in WAT. Once it is populated, we predict that its lifetime is longer in WAT than in non HB solvents. Solvent thus affects dCyd excited state decay mainly by modulating the interplay between the dark and the bright PES; in hydrogen bonding solvents repopulation of the bright excited states from the dark ones is more difficult, and the involvement of the latter in the slower dynamics is more likely. Solvent proticity is thus more important than the static dielectric constant, as confirmed by the similar fluorescence decay found in water and methanol by Ma *et al.*²⁴ Analogously, the necessity of rearranging the solute-solvent hydrogen bond network explains why the energy barriers separating the different minima are larger in water than in non-protic solvents.

The fluorescence lifetime of 5mdCyd in ACN and WAT is extremely similar, the former being less than 10% shorter than that in WAT. 5mdCyd excited state dynamics is ruled by the energy barrier towards Eth-CoIn, which, according to our calculations, is very similar in both solvents. The slightly shorter lifetime in ACN could be explained by the red-shifted absorption spectrum; at the same excitation wavelength the initial excess of energy is larger in ACN than in WAT; the WP has thus a larger kinetic energy, helping to overcome the energy barrier.

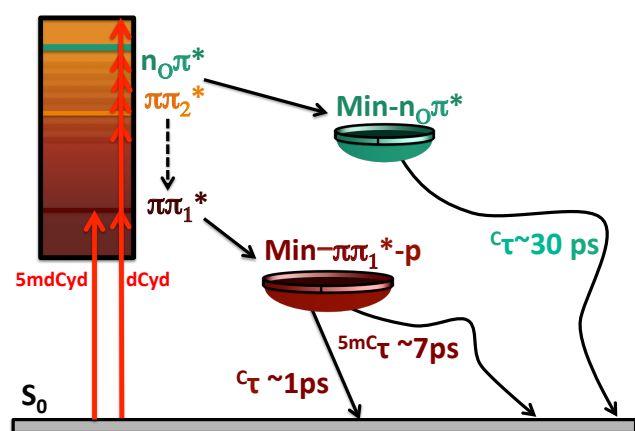


Figure 7. General Scheme for the possible deactivation mechanisms and experimental lifetimes in dCyd and 5mdCyd in WAT.

5. CONCLUSIONS

In the present study, by combining FU experiments and QM calculations we provide for the first time a general and comprehensive mechanistic description of the excited state decay of dCyd and 5mdCyd in different solvents. Our experimental results have shown that the dynamics of the bright states of dCyd and 5mdCyd is less sensitive to solvent proticity compared to uracil derivatives. According to our picture, summarized in Figure 7, the four lowest energy excited states -two bright ($\pi\pi_1^*$ and $\pi\pi_2^*$) and two dark ($n_N\pi^*$ and $n_o\pi^*$) are strongly vibronically coupled in the FC region. Independently of the solvent, the main ultrafast decay route involve $\pi\pi_1^*$ and the ethene-like CoIn. This path is almost barrierless for dCyd and provides a small energy barrier for 5mdCyd, explaining the longer lifetime and the larger fluorescence quantum yield recorded for 5mdCyd. The bright excited state, $\pi\pi_2^*$, which is noticeably populated in the FC

region, is predicted to decay either to $\pi\pi_1^*$, possibly accounting for the slower ultrafast decay in dCyd, or to act as doorway state for $n_o\pi^*$. Comparison between the computed ESA and TR-IR spectra and their experimental counterpart allows identifying in $n_o\pi^*$ the dark state experiments shown to be populated in protic solvents.²⁴ Although in WAT $n_o\pi^*$ is significantly less stable than $\pi\pi_1^*$ and $\pi\pi_2^*$, our calculations show a significant mixing with the bright excited states (much larger than that found for $n_N\pi^*$), suggesting a larger coupling and that $n_o\pi^*$ state can be populated in dCyd already in the proximity of the FC region. $n_o\pi^*$ minimum is very stable with respect to either decay to the GS or to repopulate other minima, and then accounts for the tens of ps signal in TA and TIR spectra. On the opposite $n_N\pi^*$ is not predicted to be significantly involved in the slower dynamics, but, in non protic solvents, could contribute to a slight slowing down of the sub-ps features.

Methylation at position C5 decreases the probability of populating dark states, increasing the population of $\pi\pi_1^*$ and, as discussed above, its lifetime. Since $\pi\pi_1^*$ contributes to the exciton giving rise to cyclobutane pyrimidine dimers (CPD) formation,³² these two features could play a role in the well-known larger photochemical reactivity of 5mdCyd towards CPD formation.

Considering the good agreement between the pictures provided by two very different computational approaches, our static calculations provide, together with the computed ESA and TR-IR spectra, a consistent framework for the interpretation of the TR experiments. On the other hand, it is clear that excited state molecular dynamic simulations would be fundamental to fully elucidate the details of the photoactivated dynamics of dCyd in solution and to provide a direct comparison with the TR-experiments. In this respect, the present study shows that dCyd pose huge difficulties to dynamical calculations, due to the large number of excited states to be considered on the same foot, the significant vibronic coupling among them, the strong dependence on the adopted electronic method and the necessity of a reliable inclusion of dynamical solvation effects.

By assessing all the most relevant open issues concerning the excited state decay of dCyd and 5mdCyd, this study also provides a solid ground for understanding the behavior of these bases in DNA single and double strands.

ASSOCIATED CONTENT

Supporting Information

Experimental and computational details, additional computational results, further analysis of the Frank-Condon Region and the different connective pathways together with the study of the sugar effect into the main deactivation pathways can be found in the Supporting Information.

The Supporting Information is available free of charge on the ACS Publications website.

AUTHOR INFORMATION

Present Addresses

*School of Chemistry, University of East Anglia, Norwich Research Park, NR4 7TJ, Norwich, United Kingdom

Corresponding Author

*akos.banyasz@cea.fr

*marco.garavelli@unibo.it

*robimp@unina.it

ACKNOWLEDGMENT

R. I. thanks CNR, Progetto Bilaterale CNR/CNRS PICS 2015 and the French Agency Research Grant ANR-12-BS08-0001-01 for financial support. L. M.-F. acknowledges the LR. Campania num 5/2002- Annualità 2007.

M.G. acknowledges support by the European Research Council Advanced Grant STRATUS (ERC-2011-AdG No. 291198) and of the French Agence National de la Recherche (FEMTO-2DNA, ANR-15-CE29-0010). J.S.-M. acknowledges Project No. CTQ2014-58624-P of the Spanish MINECO (Ministerio de Economía y Competitividad). Sean Dingemans is acknowledged for his contributions in the early stages of the project.

A. B., D. M., T. G. and J. J. acknowledges the support of the international scientific cooperation project PICS n° 6827 and the French Agency for Research (ANR-12-BS08-0001-01). J.J. acknowledges the support of the Erasmus+ programme of the European Union.

- (1) Cadet, J.; Vigny, P. In *Bioorganic Photochemistry*; Morrison, H., Ed.; John Wiley & Sons: New York, 1990, p 1.
- (2) Gustavsson, T.; Improt, R.; Markovitsi, D. *J. Phys. Chem. Lett.* **2010**, *1*, 2025.
- (3) Crespo-Hernández, C. E.; Cohen, B.; Hare, P. M.; Kohler, B. *Chem. Rev.* **2004**, *104*, 1977.
- (4) Improt, R.; Santoro, F.; Blancafort, L. *Chem. Rev.* **2016**, *116*, 3540.
- (5) Giussani, A.; Segarra-Martí, J.; Roca-Sanjuán, D.; Merchán, M. In *Photoinduced Phenomena in Nucleic Acids I: Nucleobases in the Gas Phase and in Solvents*; Barbatti, M., Borin, C. A., Ullrich, S., Eds.; Springer International Publishing: Cham, 2015; Vol. 355, p 57.
- (6) Barbatti, M.; Aquino, A. J.; Szymczak, J. J.; Nachtigallova, D.; Hobza, P.; Lischka, H. *Proc. Natl. Acad. Sci. USA* **2010**, *107*, 21453.
- (7) Mai, S.; Richter, M.; Marquetand, P.; González, L. In *Photoinduced Phenomena in Nucleic Acids I: Nucleobases in the Gas Phase and in Solvents*; Barbatti, M., Borin, C. A., Ullrich, S., Eds.; Springer International Publishing: Cham, 2015; Vol. 355, p 99.
- (8) Middleton, C. T.; de La Harpe, K.; Su, C.; Law, Y. K.; Crespo-Hernández, C. E.; Kohler, B. *Annu. Rev. Phys. Chem.* **2009**, *60*, 217.
- (9) Markovitsi, D.; Gustavsson, T.; Vayá, I. *J. Phys. Chem. Lett.* **2010**, *1*, 3271.
- (10) Avila Ferrer, F. J.; Santoro, F.; Improt, R. *Comput. Theor. Chem.* **2014**, *1040–1041*, 186.
- (11) Blancafort, L. *Photochem. and Photobiol.* **2007**, *83*, 603.
- (12) Blancafort, L.; Migani, A. *J. Photochem. and Photobiol. A: Chem.* **2007**, *190*, 283.
- (13) Kistler, K. A.; Matsika, S. *J. Phys. Chem. A* **2007**, *111*, 8708.
- (14) Merchán, M.; Serrano-Andrés, L. *J. Am. Chem. Soc.* **2003**, *125*, 8108.
- (15) Kistler, K. A.; Matsika, S. *J. Chem. Phys.* **2008**, *128*, 215102.
- (16) Barbatti, M.; Aquino, A. J. A.; Szymczak, J. J.; Nachtigallova, D.; Lischka, H. *Phys. Chem. Chem. Phys.* **2011**, *13*, 6145.
- (17) González-Vázquez, J.; González, L. *Chem. Phys. Chem.* **2010**, *11*, 3617.
- (18) Sebastian, M.; Marquetand, P.; Richter, M.; González-Vázquez, J.; González, L. *Chem. Phys. Chem.* **2013**, *14*, 2920.
- (19) Hudock, H. R.; Martínez, T. J. *ChemPhysChem* **2008**, *9*, 2486.
- (20) Ismail, N.; Blancafort, L.; Olivucci, M.; Kohler, B.; Robb, M. A. *J. Am. Chem. Soc.* **2002**, *124*, 6818.
- (21) Blaser, S.; Trachsel, M. A.; Lobsiger, S.; Wiedmer, T.; Frey, H.-M.; Leutwyler, S. *J. Phys. Chem. Lett.* **2016**, *7*, 752.
- (22) Keane, P. M.; Wojdyla, M.; Doorley, G. W.; Watson, G. W.; Clark, I. P.; Greetham, G. M.; Parker, A. W.; Towrie, M.; Kelly, J. M.; Quinn, S. J. *J. Am. Chem. Soc.* **2011**, *133*, 4212.
- (23) Quinn, S.; Doorley, G. W.; Watson, G. W.; Cowan, A. J.; George, M. W.; Parker, A. W.; Ronayne, K. L.; Towrie, M.; Kelly, J. M. *Chem. Commun.* **2007**, 2130.
- (24) Ma, C.; Cheng, C. C.-W.; Chan, C. T.-L.; Chan, R. C.-T.; Kwok, W.-M. *Phys. Chem. Chem. Phys.* **2015**, *17*, 19045.
- (25) Malone, R. J.; Miller, A. M.; Kohler, B. *Photochem. Photobiol.* **2003**, *77*, 1751.
- (26) Rottger, K.; Marroux, H. J. B.; Bohnke, H.; Morris, D. T. J.; Voice, A. T.; Temps, F.; Roberts, G. M.; Orr-Ewing, A. J. *Faraday Discussions* **2016**.
- (27) Chatterley, A. S.; West, C. W.; Stavros, V. G.; Verlet, J. R. R. *Chem. Sci.* **2014**, *5*, 3963.
- (28) Holliday, R.; Pugh, J. E. *Science* **1975**, *187*, 226.
- (29) Lister, R.; Ecker, J. R. *Genome Res.* **2009**, *19*, 959.
- (30) Smith, Z. D.; Meissner, A. *Nat Rev Genet* **2013**, *14*, 204.
- (31) Sharonov, A.; Gustavsson, T.; Marguet, S.; Markovitsi, D. *Photochem. Photobiol. Sci.* **2003**, *2*, 362.
- (32) Esposito, L.; Banyasz, A.; Douki, T.; Perron, M.; Markovitsi, D.; Improt, R. *J. Am. Chem. Soc.* **2014**, *136*, 10838.
- (33) Banyasz, A.; Esposito, L.; Douki, T.; Perron, M.; Improt, R.; Markovitsi, D. *J. Phys. Chem. B* **2016**, *120*, 4232.
- (34) Baylin, S. B. *Nat. Clin. Prac. Oncol.* **2005**, *2*, S4.
- (35) Baylin, S. B.; Jones, P. A. *Nat. Rev. Cancer* **2011**, *11*, 726.
- (36) Tommasi, S.; Denissenko, M. F.; Pfeifer, G. P. *Cancer Res.* **1997**, *57*, 4727.
- (37) Denissenko, M. F.; Chen, J. X.; Tang, M.-S.; Pfeifer, G. P. *Proc. Natl. Acad. Sci. USA* **1997**, *94*, 3893.
- (38) Gustavsson, T.; Sarkar, N.; Lazzarotto, E.; Markovitsi, D.; Improt, R. *Chem. Phys. Lett.* **2006**, *429*, 551.
- (39) Nakayama, A.; Yamazaki, S.; Taketsugu, T. *J. Phys. Chem. A* **2014**, *118*, 9429.
- (40) Li, Q.; Blancafort, L. *Photochem. Photobiol. Sci.* **2013**, *12*, 1401.

- (41) Blancafort, L.; Cohen, B.; Hare, P. M.; Kohler, B.; Robb, M. A. *J. Phys. Chem. A* **2005**, *109*, 4431.
- (42) Lobsiger, S.; Trachsel, M. A.; Frey, H.-M.; Leutwyler, S. *The Journal of Physical Chemistry B* **2013**, *117*, 6106.
- (43) Kistler, K. A.; Matsika, S. *J. Phys. Chem. A* **2007**, *111*, 2650.
- (44) Tomić, K.; Tatchen, J.; Marian, C. M. *J. Phys. Chem. A* **2005**, *109*, 8410.
- (45) Trachsel, M. A.; Wiedmer, T.; Blaser, S.; Frey, H.-M.; Li, Q.; Ruiz-Barragan, S.; Blancafort, L.; Leutwyler, S. *J. Chem. Phys.* **2016**, *145*, 134307.
- (46) Kistler, K. A.; Matsika, S. *J. Phys. Chem. A* **2009**, *113*, 12396.
- (47) Li, Q.; Mennucci, B.; Robb, M. A.; Blancafort, L.; Curutchet, C. *J. Chem. Theor. Comput.* **2015**, *11*, 1674.
- (48) Tomasi, J.; Mennucci, B.; Cammi, R. *Chem. Rev.* **2005**, *105*, 2999.
- (49) Miertuš, S.; Scrocco, E.; Tomasi, J. *Chem. Phys.* **1981**, *55*, 117.
- (50) Pollum, M.; Martínez-Fernández, L.; Crespo-Hernández, C. E. In *Photoinduced Phenomena in Nucleic Acids I: Nucleobases in the Gas Phase and in Solvents*; Barbatti, M., Borin, C. A., Ullrich, S., Eds.; Springer International Publishing: Cham, 2015; Vol. 355, p 245.
- (51) Görner, H. *J. Photochem. Photobiol. B* **1990**, *5*, 359.
- (52) Nikogosyan, D. N.; Angelov, D. A.; Oraevsky, A. A. *Photochem. Photobiol.* **1982**, *35*, 627.
- (53) Onidas, D.; Markovitsi, D.; Marguet, S.; Sharonov, A.; Gustavsson, T. *J. Phys. Chem. B* **2002**, *106*, 11367.
- (54) Miannay, F.-A.; Gustavsson, T.; Banyasz, A.; Markovitsi, D. *J. Phys. Chem. A* **2010**, *114*, 3256.
- (55) Gustavsson, T.; Bányász, Á.; Lazzarotto, E.; Markovitsi, D.; Scalmani, G.; Frisch, M. J.; Barone, V.; Improta, R. *J. Am. Chem. Soc.* **2006**, *128*, 607.
- (56) Frisch, M. J. *et al Gaussian 09, Revision A.1, in, Gaussian, Inc., Wallingford CT* **2009**.
- (57) Case, D. A.; Darden, T. A.; Cheatham, T. E.; Simmerling, C. L.; Wang, J.; Duke, R. E.; Luo, R.; Walker, R. C.; Zhang, W.; Merz, K. M. *Amber 11*, University of California, 2010.
- (58) Wang, J.; Cieplak, P.; Kollman, P. A. *J. Comput. Chem.* **2000**, *21*, 1049.
- (59) Jorgensen, W. L.; Chandrasekhar, J.; Madura, J. D.; Impey, R. W.; Klein, M. L. *J. Chem. Phys.* **1983**, *79*, 926.
- (60) Senn, H. M.; Thiel, W. In *Atomistic Approaches in Modern Biology: From Quantum Chemistry to Molecular Simulations*; Reiher, M., Ed.; Springer Berlin Heidelberg: Berlin, Heidelberg, 2007, p 173.
- (61) Andersson, K.; Malmqvist, P. Å.; Roos, B. O. *J. Chem. Phys.* **1992**, *96*, 1218.
- (62) Roca-Sanjuán, D.; Aquilante, F.; Lindh, R. *Wiley Interdisciplinary Reviews: Computational Molecular Science* **2012**, *2*, 585.
- (63) Finley, J.; Malmqvist, P. Å.; Roos, B. O.; Serrano-Andrés, L. *Chem. Phys. Lett.* **1998**, *288*, 299.
- (64) Altoè, P.; Stenta, M.; Bottoni, A.; Garavelli, M. *Theor. Chem. Acc.* **2007**, *118*, 219.
- (65) Aquilante, F.; Autschbach, J.; Carlson, R. K.; Chibotaru, L. F.; Delcey, M. G.; De Vico, L.; Fdez. Galván, I.; Ferré, N.; Frutos, L. M.; Gagliardi, L.; Garavelli, M.; Giussani, A.; Hoyer, C. E.; Li Manni, G.; Lischka, H.; Ma, D.; Malmqvist, P. Å.; Müller, T.; Nenov, A.; Olivucci, M.; Pedersen, T. B.; Peng, D.; Plasser, F.; Pritchard, B.; Reiher, M.; Rivalta, I.; Schapiro, I.; Segarra-Martí, J.; Stenrup, M.; Truhlar, D. G.; Ungur, L.; Valentini, A.; Vancollie, S.; Veryazov, V.; Vysotskiy, V. P.; Weingart, O.; Zapata, F.; Lindh, R. *J. Comput. Chem.* **2016**, *37*, 506.
- (66) Martínez-Fernández, L.; Pepino, A. J.; Segarra-Martí, J.; Banyasz, A.; Garavelli, M.; Improta, R. *J. Chem. Theor. Comput.* **2016**, *12*, 4430.
- (67) Blancafort, L.; Robb, M. A. *J. Phys. Chem. A* **2004**, *108*, 10609.
- (68) Canuel, C.; Mons, M.; Piuze, F.; Tardivel, B.; Dimicoli, I.; Elhanine, M. *J. Chem. Phys.* **2005**, *122*, 074316.
- (69) Ullrich, S.; Schultz, T.; Zgierski, M. Z.; Stolow, A. *Phys. Chem. Chem. Phys.* **2004**, *6*, 2796.
- (70) Kosma, K.; Schröter, C.; Samoylova, E.; Hertel, I. V.; Schultz, T. *J. Am. Chem. Soc.* **2009**, *131*, 16939.
- (71) Nakayama, A.; Harabuchi, Y.; Yamazaki, S.; Taketsugu, T. *Phys. Chem. Chem. Phys.* **2013**, *15*, 12322.